JJMIE

Volume 19, Number 1, March. 2025
ISSN 1995-6665
Pages 237– 248
https://doi.org/10.59038/jjmie/190119
Editor-in-Chief: Prof. Ali M. Jawarneh

Jordan Journal of Mechanical and Industrial Engineering

Diagnosis of Hydrodynamic Bearings by Evaluation based on Orbital Analysis Approach

Imad El Adraoui [1,3*], Youssef Jabari [2], Hassan Gziri [2,3]

[1] Materials, Systems and Energy Engineering Laboratory (MaSEEL), Faculty of Sciences and Technology, Abdelmalek Essaadi University, Tangier, Morocco
[2] Laboratory of Engineering, Industrial Management, and Innovation (IMII), Faculty of Sciences and Technology, Hassan 1st University, Settat, Morocco
[3] Laboratory of Engineering and Innovation of Advanced Systems (LIISA), Faculty of Sciences and Technology, Hassan 1st University, Settat, Morocco.

Received 13 Nov 2024 *Accepted 12 Jan 2025*

Abstract

The evaluation and diagnosis of rotating machines rely on several approaches. However, for a complex system or in the presence of several faults, these approaches become less robust, less accurate, and less reliable. To address these shortcomings, this paper proposes a diagnostic approach for hydrodynamic bearings in a rotating machine based on orbital analysis. This approach requires piezoelectric material sensors installed in the three directions: X, Y, and Z. Its objective is to evaluate the performance of the hydrodynamic bearing by comparing the collected data with the ISO 7919-5 standard. The methodology is based on data acquisition using several sensors measuring the displacements of the shaft line. Then, the results are analyzed according to the indicators required by ISO 7919-5, such as: S_{max}, S_{pp}, S_{p1}, S_{p2}, eccentricity, and barycenter G along X and Y. The shaft line displacement orbits make it possible to assess the health of the hydrodynamic bearing and identify possible defects. Finally, the proven results of this approach provide an accurate and efficient diagnosis of the operating state. The approach used has demonstrated a good assessment and a relevant diagnosis. This validates its ability to implement it in future research work, such as the diagnosis of complex rotating machines, mechanical systems in the presence of several defects, and the exploitation of this data in real time in the prediction of mechanical defects by the implementation of an expert system.

Keywords: Diagnosis, Orbital analysis, Shaft line, Hydrodynamic bearing, Piezoelectric sensor.

Acronyms and Symbols

3D-IOM	Three-Dimensional Instantaneous Orbit Map;
CEEMD	Complementary Ensemble Empirical Mode Decomposition;
CNN	Convolutional Neural Network;
IAS	Instantaneous Angular Speed;
LSTM	Long-Short-Term Memory;
PAI, PAS, and PTU	Lower and Upper Alternator Bearings, Turbine Bearing (Respectively);
MCVMD	Multivariate Complex Variational Mode Decomposition;
MVMD	Multivariate Variational Mode Decomposition;
MOMEDA	Modified Orthogonal Minimum Entropy Deconvolution Algorithm;
VMD	Variational Mode Decomposition;
dW_x and dW_y	Elementary force along the x and y axis (Respectively);
W_x and W_y	Force along the x and y axis (Respectively);
R, R_a, θ, φ, X_a, Y_a, y, OO_a, and z	Geometric parameters;
p, p_l	Any point pressure and lubricant pressure (Respectively);
ω	Rotation frequency;
τ_{xy}	Shear stress in the Oxy plane;
μ	Dynamic viscosity of the lubricant;
u	Displacement of one lubricant layer relative to another;
A_{xx}, A_{xy}, A_{yx}, and A_{yy}	Stiffness coefficients according to the different orientations;
$\dot{x}$, $\dot{y}$	Speeds at the center of the shaft according to the axis x and y (Respectively);
T	Period of movement;
C_b	Radial clearance;
Λ	Compressibility number;
t	Time

* Corresponding author e-mail: aimadeladraoui@gmail.com.

1. Introduction

Bearings are considered an important element for the efficient operation of rotating machinery; they provide stability and support to rotating shafts. However, each bearing failure can lead to unplanned and costly downtime [1]. Therefore, bearing monitoring has become one of the top priorities to ensure the reliability and performance of rotating machinery. Because it falls within the framework of total productive maintenance (TPM) to ensure quality and availability [2], then adopt advanced technology to implement the notion of monitoring and Industry 4.0 [3]. The monitoring is based on a novel bearing diagnostic approach that focuses on the orbital analysis of the shaft line. By measuring and understanding the orbital displacements of the shaft line, it is possible to characterize and identify potential bearing defects, thus providing a very accurate approach for the health assessment of rotating machinery [4 , 5].

In this sense, several research works are being addressed to develop advanced bearing diagnostic approaches by exploiting the different methods of analyzing the data collected by installed sensors. The objective of this research is to improve the accuracy and quality of shaft line orbital analysis techniques to enable highly accurate and preventive detection of bearing anomalies, optimize predictive maintenance, increase bearing life, and reduce operational costs related to unplanned downtime of industrial systems [6]. Yan et al. present a novel multi-sensor data fusion learning mechanism for detecting bearing faults [7]. They use five sensors to measure bearing displacement, then construct generalized shaft orbits converted into discrete 2D images. A convolutional neural network is then used to extract discriminative features from 2D images, thus making it possible to classify defect types. Experiments carried out on an installation with bearings support the effectiveness of the proposed algorithm, confirming its relevance even in the case of changes in rotational speeds and sample lengths. Bruand et al. were interested in the use of Instantaneous Angular Speed (IAS) in the condition monitoring of rotating machines [8]. Their objective was to establish a study of the mechanical faults involved in these rotating machines by combining the IAS variations with torque anomalies in the case of the presence of a mechanical fault, namely the bearing breakage as an example. This study gives a relevant point of view on the measurement of the IAS by establishing a relationship between the vibrations of the shaft line and the IAS variations. Initially, they examined the orbit of a rotating shaft to demonstrate that it contained relevant information about the health of the bearing. Then, they combined angular position sensors to reconstruct this orbit. The results showed that IAS measurements are sensitive to shaft vibrations, which can improve diagnostic capabilities. Furthermore, the researchers proposed an analytical method based on the linearization of the JB force and generalized eigenvalue analysis to predict the stability of synchronous vibrations in vertical rotating shaft systems. This extended analysis of the eigenvalues makes it possible to directly determine the stability of the synchronous orbit. A method is used to feed rotor dynamics software, calculating the stability thresholds of rotating shaft bearings [9]. Moreover, the researchers addressed the problem of the machining deviation of the positioning hole of the inter-shaft bearing, which may lead to the non-concentricity defect of the double rotor system [10]. They identified this problem as a type of parallel nonconcentricity, characterized by phase angle and offset, used to adjust the contact force model of the intershaft bearing. Their results showed that these parameters change the amplitude when the dual-rotor system exceeds the first critical speed. They also observed 2X and 3X frequencies of the rotational speeds of the high and low pressure rotors, as well as several combined frequencies of the two rotational speeds, where the subtraction frequency of the high and low pressure rotors is dominant. In addition, the non-concentricity phase angle variations, with respect to the shaft line, have a direct influence on the shape and envelope of the orbits of the rotating parts for low and high pressure. These proven results ensure the importance of considering geometric changes in the design and analysis of dual-rotor machines to ensure their stability and good working condition. Jiang et al. proposed an innovative learning model, called Orbit LSTM, to monitor the health of turbomachinery by modeling dynamic behaviors based on multiple image sequences of the orbits [11]. This model combines the convolutional long short-term memory (LSTM) network with the capability of a convolutional neural network (CNN) to automatically extract features from these images. It is trained and built based on a sequence of images of orbits in good working condition. The fusion of CNN and LSTM capabilities allows obtaining long-term memory in the behaviors of sequences archived in history.

Ma et al. developed a semi-active suspension (SAS) system with nonlinear hydraulic adjustable damper (HAD) that improves performance through multi-objective control based on fuzzy neural network [12]. The model accuracy and reliability are proven in terms of real-time fault tracking and early warning using vibration signals collected and simulated data from different industrial turbomachines. This method provides an approach for accurate fault detection in predictive maintenance of turbomachines, focusing the innovative importance of machine learning approaches in the axis that deals with industrial machine monitoring. A presented study focuses on high-resolution spectrum analysis [13], aiming to calculate the amplitude, frequency, and phase details of sinusoidal harmonic and subharmonic vibrations in large rotating machines. From this high-resolution spectrum, a purified tree orbit is reconstructed to remove interference terms. The properties of the curves and instantaneous times, which are insensitive to translational scale changes and shaft orbit rotation, are then used to extract the refined vibrational orbit characteristics. Subsequently, this charter has proven to be effective in diagnosing various anomalies affecting gas turbines, covering different operating conditions and start-up stages. The approach introduces a reliable method for analyzing and detecting problems associated with these rotating machines, also specifying its importance in ensuring their performance and reliability. The authors addressed the examination of lateral vibrations in a nonlinear and asymmetric rotating shaft system with vertical support mechanism [14]. They used four-pole active magnetic bearing equipment as an actuator for

applying magnetic forces. The latter have the possibility to control them in order to stabilize the equipment studied. Based on the conclusion of this research work, which is a mathematical model aimed at controlling the dynamics of the system, the researchers obtained equations for the slow flow of motion based on asymptotic analysis. The oscillatory behaviors of the system were studied before and after the application of the control. The main results revealed that the asymmetric rotating shaft system, without control, could exhibit significant amplitudes. Finally, the conditions to avoid the occurrence of friction or impact force between the rotating shaft and the legs of the electromagnetic pole were discussed. This research study investigates the importance of active control in vibration reduction and stabilization of rotating equipment systems, which offers prospects for improving some of their important characteristics, such as reliability and performance. The paper [15] introduces multivariate variational mode decomposition (MVMD) and complex-valued signal decomposition. Cui et al. proposed multivariate complex variational mode decomposition (MCVMD), an approach with the ability to extract the different forward and reverse components of multiple bearing sections, as well as to perform a non-stationary complex-type decomposition of the rotating part signal. An analysis of the tribological behaviour of a ZA27 hybrid composite was treated for the ZA27 hybrid composite with SiC and graphite as addition elements [16]. Then, a characterization of the wear degradation of ZA27 zinc-aluminium alloy [17]. A qualitative analysis of the lubrication of porous sliding bearings can also be found in [18], Marinković et al. established a model that aims to analyze the lubricant behavior under various conditions. For the purpose of health monitoring, they also presented three-dimensional instantaneous orbit analysis (3D-IOM), the latter allowing a fairly in-depth analysis of shaft vibrations and providing a new method for signal fusion of rotating machine bearings. This treated methodology has remarkable importance in improving to understand the behavior and monitor rotating machines by giving innovative vibration analysis techniques.

Some other recent advances in fault diagnosis use advanced signal processing and machine learning techniques for reliability improvement in different applications. Shen et al. present an enhanced complementary ensemble empirical mode decomposition (CEEMD) combined with a modified orthogonal minimum entropy deconvolution (MOMEDA) algorithm for the purpose of efficient diagnosis of axlebox bearing faults in rotating equipment, demonstrating remarkable innovations in accuracy [19]. Boussouloub et al. propose a new approach based on the use of variational mode decomposition (VMD) [20], which develops bearing fault detection by isolating the relevant frequency components and finally demonstrating the effectiveness under different operating conditions [21]. As well as Lakikza et al. focus on rotating mechanisms of wind turbines, by integrating vibration signal processing with machine learning, in order to identify bearing defects, aiming at the importance of these approaches in the field of renewable energy [22].Xue et al. studied the effectiveness of the approach based on the use of torsional vibration signals, knowing that it is a powerful tool for the detection of defects affecting the planetary bearing [23]. Chen et al. propose an approach to identify wear parameters in hydrodynamic bearings based on on-rotor sensing (ORS) technology and operational modal analysis (OMA) [24]. Still in the context of hydrodynamic bearings, the tribological context discussed in [25] comes into play to examine the lubricant effect and rheological behavior, behavior analysis by wear [26] with ANOVA Taguchi [27-29].

According to the treated state of the art, several approaches are presented to highlight the diagnosis of hydrodynamic bearings. Each treated approach has limitations, such as the limitation of the management of the variability of the operating conditions of the system, the noises in the data, the complexity of interpretation of the results, and the robustness problem for a dynamic system subjected to several faults. The approach proposed in this work is used to develop diagnostic techniques for hydrodynamic bearings by orbital analysis of shaft line displacements. With emphasis on their important role in predictive maintenance and operational efficiency. It presents an improvement in robustness under variable operating conditions in the presence of several faults addressed in [30], with real-time data collection with high-precision piezoelectric sensors and negligible noise. Therefore, this work is organized as follows:

- Formalism of the model associated with the hydrodynamic bearing;
- Material and method;
- Results and discussion.

2. Formulation of Model

This section presents a brief description of the model formulation. The value of the force exerted by the lubricant film on the shaft is calculated by integrating the pressure field obtained throughout the lubricant film. We define a reference frame OX_aY_a, with the axis OX_a carried by the line of centers OO_a. A point M of the bearing is identified by the angle θ (see Figure 1).

The components of the elementary force applied by the lubricant film in M are then written according to formulas (1) and (2) [31, 32]:

$$dW_x = (p - p_l)R.d\theta.dz\cos\theta \quad (1)$$

$$dW_y = (p - p_l)R.d\theta.dz\sin\theta \quad (2)$$

and therefore, the components of the action of the lubricant film on the shaft are expressed as follows by formulas (3) and (4) :

$$W_x = \int_{\theta_{\min}}^{\theta_{\max}} \int_0^L (p - p_l)R.d\theta.dz\cos\theta \quad (3)$$

$$W_y = \int_{\theta_{\min}}^{\theta_{\max}} \int_0^L (p - p_l)R.d\theta.dz\sin\theta \quad (4)$$

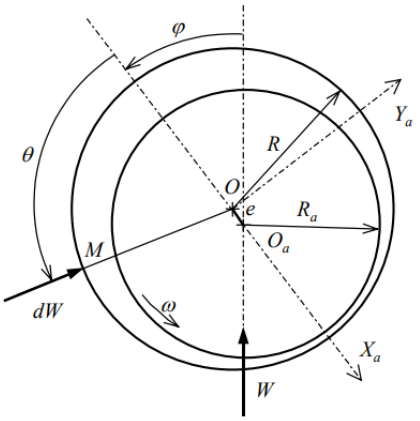

Figure 1. Geometric model of the bearing.

The calculation of the fluid friction torque is carried out on one or other of the walls of the contact (shaft or bearing) by integration of the shear stress. The expression of the shear stress that interests us is expressed by formula (5) [32]:

$$\tau_{xy} = \mu \frac{\partial u}{\partial y} = \frac{1}{2R}\frac{\partial p}{\partial \theta}(2y-h) + \frac{\mu}{h} R\omega \tag{5}$$

The center of the shaft is moved parallel to the OX and OY axes of $\pm\Delta X$ and $\pm\Delta Y$. The value of these displacements is chosen as a relative value compared to the radial clearance. This value is generally found in [4], and the results obtained are satisfactory. However, we will present a study of the influence of the choice of the value of the disturbances on the terms of the stiffness matrix [33]. The stiffness coefficients are then written as a function of the lifts calculated following the disturbances according to OX and OY by the following formulas (6), (7), (8), and (9):

$$A_{xx} = -\frac{W_x(\Delta X) - W_x(-\Delta X)}{2\Delta X} \tag{6}$$

$$A_{xy} = -\frac{W_x(\Delta Y) - W_x(-\Delta Y)}{2\Delta Y} \tag{7}$$

$$A_{yx} = -\frac{W_y(\Delta X) - W_y(-\Delta X)}{2\Delta X} \tag{8}$$

$$A_{yy} = -\frac{W_y(\Delta Y) - W_y(-\Delta Y)}{2\Delta Y} \tag{9}$$

The damping coefficients are expressed according to [32, 33] by formula (10) as follows:

$$\begin{pmatrix} \Delta W_x \\ \Delta W_y \end{pmatrix} = -\begin{bmatrix} B_{xx} & B_{xy} \\ B_{yx} & B_{yy} \end{bmatrix} \begin{pmatrix} \dot{x} \\ \dot{y} \end{pmatrix} \tag{10}$$

The principle is similar to that applied for calculating the stiffness matrix. We impose movement speeds at the center of the shaft $\pm\Delta\dot{X}$ and $\pm\Delta\dot{Y}$ (reference linked to the load). The introduction of these fluctuations in speed modifies the Reynolds equation. Using the expression for the components of the surface velocities, we can write the time-dependent Reynolds formula (11) as follows [32]:

$$\frac{\partial}{\partial\theta}\left[PH^3\frac{\partial P}{\partial\theta}\right] + \frac{\partial}{\partial Z}\left[PH^3\frac{\partial P}{\partial Z}\right] = \Lambda\frac{\partial(PH)}{\partial\theta} + 2\Lambda\frac{\partial(PH)}{\partial T} \tag{11}$$

Parameters in capital letters are dimensionless:

$P = \frac{p}{p_l}$, $H = \frac{h}{C_b}$, $Z = \frac{z}{R_a}$, *and* $T = t\omega$ with: p_l pressure lubricant.

The principle is to move the center of the tree of $\pm\Delta X$ and $\pm\Delta Y$ values, considering that these movements take place during a unit time. The calculation of the $\frac{\partial(PH)}{\partial T}$ term involves variations in the pressure and height fields as a function of time. The variation in height is calculated by the difference in the height field at equilibrium and the height field after the movement of the tree. On the other hand, for the variation of the pressure field, the calculation is carried out during the resolution of the Reynolds equation by the iterative Newton-Raphson process [34].

The eccentricity of the shaft is no longer sufficient to define lift. It is necessary to take into account the number Λ called the compressibility number [35]. It depends on the dynamic viscosity of the lubricating fluid μ, the rotation speed of the shaft ω, the radial clearance C_b, and the pressure p [31](see formula (12)).

$$\Lambda = \frac{6\mu\omega}{p}\left(\frac{R_a}{C_b}\right)^2 \tag{12}$$

The convergence is achieved when the rotor trajectory is stabilized on an orbit [32, 33]. Given the periodic nature of the movement, the iteration stopping test is expressed by formula (13):

$$\sqrt{\left[\frac{X(t)-X(t+T)}{X(t)}\right]^2 + \left[\frac{Y(t)-Y(t+T)}{Y(t)}\right]^2} \le C_b \tag{13}$$

with T the period of movement.

3. Material and Method

This section presents the equipment used for data collection and analysis in this study. Three bearings are used: (PTU), (PAI), and (PAS). Each of these bearings offers distinct characteristics that allow for the evaluation of different aspects of the mechanisms studied. For the collection of displacement data, piezoelectric sensors are installed on the bearings (see Figures 2, 3, and 4) arranged in three distinct directions. These sensors are essential to accurately measure the displacements and vibrations of the tested mechanisms.

The approach proposed in this paper includes a set of essential steps. First, prepare a precise experimental protocol to collect data related to the studied system in real time, based on the use of piezoelectric sensors (see Table 1). These sensors record the placements along the specific directions, X, Y, and Z, after giving a global vision of the behavior of the system. The installation of the sensors is done at the three hydrodynamic bearings: (PTU), (PAS), and (PAI). Then, the analysis of the collected data by identifying the nature of the orbits. This analysis allowed us to determine trends and patterns in the movements of the mechanisms, as well as to identify possible anomalies or irregularities, i.e., eccentricity with respect to the shaft line (see Figure. 5). The aspect of this method is the comparison of the collected data with the values of the functional clearance allowed according to the ISO 7919-5 standard. In addition, ISO 7919-5 provides guidelines (Am, Ax, RG, and RD) and normal performance standards

for various aspects of mechanical systems. This approach also allows working on identifying areas of modification and improvement for predictive maintenance, which helps to further develop the overall performance of the hydrodynamic bearings studied.

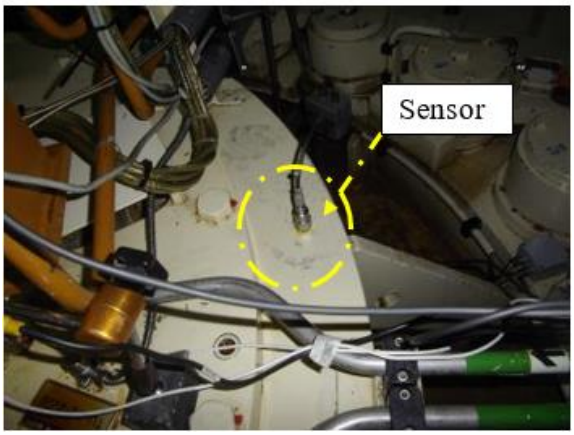

Figure 2. Sensor installation on PTU.

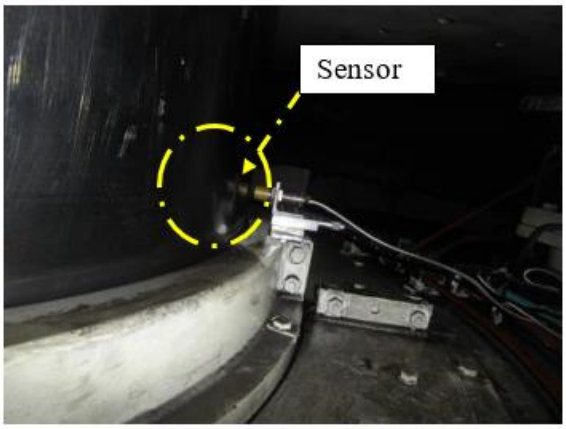

Figure 3. Sensor installation on PAI

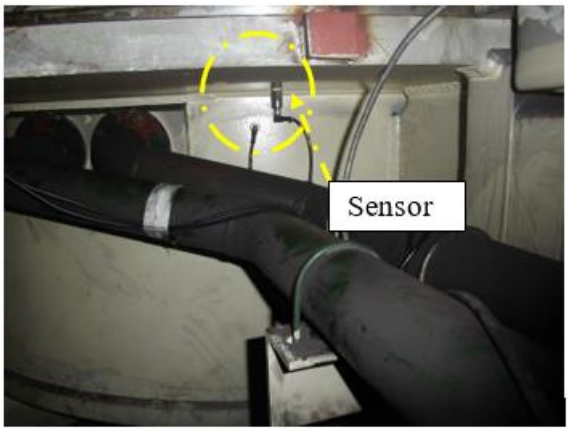

Figure 4. Sensor installation on PAS.

The test protocol is carried out according to several signatures, such as:

- Start-up to unexcited no-load operation;
- Signature in unexcited no-load operation (*MAVNE*);
- Signature in excited no-load operation (*MAVEX*);
- Signature at *20 MW* (*MQUART*);
- Signature at *40 MW* (*MDEMI*);
- Signatures at half load with supply and absorption of reagent (*MDEMI +Q / MDEMI –Q*);
- Signature at *60 MW* (*M3QUARTS*);
- Signature at full load (*MPMAX*);
- Monitoring of load drop and normal shutdown.

Table 1. Series of piezoelectric sensors used.

Designation	Type	Serial number
Analyzer	OR36	901098
Accelerometer	101.01-9-2	A3338
		A6249
		A6743
		A6744
		A6745
		A6747
		A6748
		A6749
		A6750
		A6751
Displacement sensor	TQ403	AL66351
		AL71302
		AM92422
		AM92423
		AK25315
		AK84133
Tachometer	VLS7/T/LSR	1026956
Current clamp	U 200 A / 1V	12

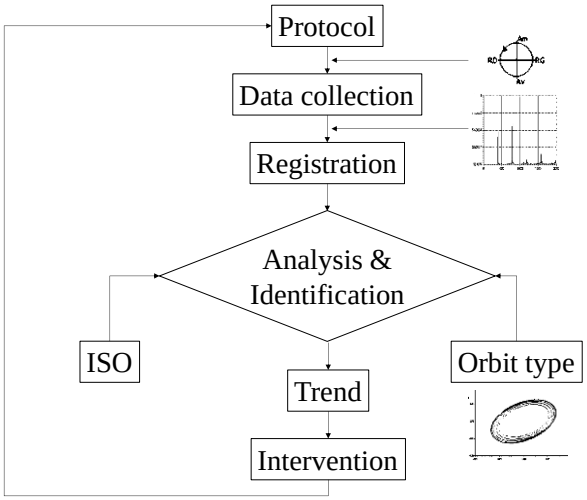

Figure 5. Proposed methodology.

Vibration data are indicators of equipment faults that can be used to design more effective fault management strategies when used in conjunction with other data sources. For rotating equipment, rotational speed, operating regime and load affect its vibration response. To ensure the safety and reliability of machinery, it is essential to protect it from mechanical vibration and ensure high availability. Modern condition monitoring systems measure noise to calculate characteristics such as vibration levels at various rotational frequencies. It is recommended to place vibration sensors near the bearings, with

additional measurements on the rotor, shaft and surrounding structure. Accelerometers are placed on the stators to detect possible structural problems. Displacement sensors must also take into account angle variations depending on the orientation of the bearings (horizontal or vertical).

ISO 7919-5 is a standard that focuses on monitoring rotating machines based on vibration analysis, by taking measurements directly on the shafts. It provides measurements on the diagnosis and evaluation of machines. It takes into account the types of sensors and their positioning, the environmental constraints (temperature, load, etc.), and the rotation frequency of the rotating machine. It evaluates the system according to zones called limit values. ISO 7919-5 norms for the peak-to-peak vibration ranges are usually used to compare vibration levels to the hydropower standards. The graph below shows that the thresholds of the mentioned norms vary based on the machine's rotation speed (rpm) (see Figure. 6).

The signals are low-pass filtered at 25 Hz, and the collected indicators are displayed in µm, such as:

- S_{max}: the greatest distance from the barycenter of the orbit;
- Excentr.: relative displacement of this barycenter during the tests;
- S_{p1}: maximum value of the orbit in the direction of probe 1;
- S_{p2}: maximum value of the orbit in the direction of probe 2;
- S_{pp}: greatest distance between two points of the orbit;
- Gap X: evolution of the barycenter reported on the X axis;
- Gap Y: evolution of the barycenter reported on the Y axis.

The shaft rotation frequency is of the order of 333 rpm; this value is determined by the system manufacturer; it corresponds to the rotation frequency F_0. The manufacturer provides the theoretical clearance of the hydrodynamic bearings, denoted C_b, as follows: The clearance of the PAS and PAI bearings is of the order of 460 µm; the clearance of the PTU bearing is of the order of 420 µm.

4. Results and Discussion

This section presents the results validated by the protocol of the methodology followed. Overall, the displacement measurements are found to be compliant with ISO 7919-5, except for the case at 40 MW, where the observed values reach 508 µm during the tests with reagent variations. This significant increase is attributable to a disturbing hydraulic phenomenon that influences the displacements of the shaft line. In accordance with ISO 7919-5, these displacements place the hydrodynamic bearing in zone D, as indicated in Table 2.

The displacements at the PTU bearing are found to be significant, with a maximum of 550 µm recorded at 40 MW. In accordance with ISO 7919-5, these displacements classify the bearing in zone D. The maximum cumulative displacement of the shaft in its bearing reaches 680 µm, thus exceeding the theoretical clearance value, as specified in Table 3.

Concerning the displacements at the PAS bearing, the S_{pp} is 351 µm, with an Smax of 184 µm recorded at maximum full load. Based on ISO 7919-5, these measurements classify the bearing in zone C. The maximum cumulative displacement of the shaft in its bearing is of the order of 360 µm and is therefore less than the theoretical clearance, as shown in Table 4.

These results highlight the importance of carefully monitoring the various rotating components as part of the bearing performance and operation analysis, which allows the detection of anomalies and potential malfunctions in order to ensure the continuous proper operation of the system.

From Figure 7 and Table 5, they clearly highlight a peak at measuring point 11 of the bearing at a frequency F_0 for a signature that is indicated by operation under a load of order 40 MW. This phenomenon presents a fluctuation of the load supported by the bearing at this generated power. The detection of this peak gives remarkable indications on the operating conditions of the rotating system; thus, it allows us to understand the associated constraints and the performances of the system at different operating conditions. This remark could be the track to guide the maintenance service towards adjustments or corrective interventions in order to optimize the efficiency and reliability of the bearing.

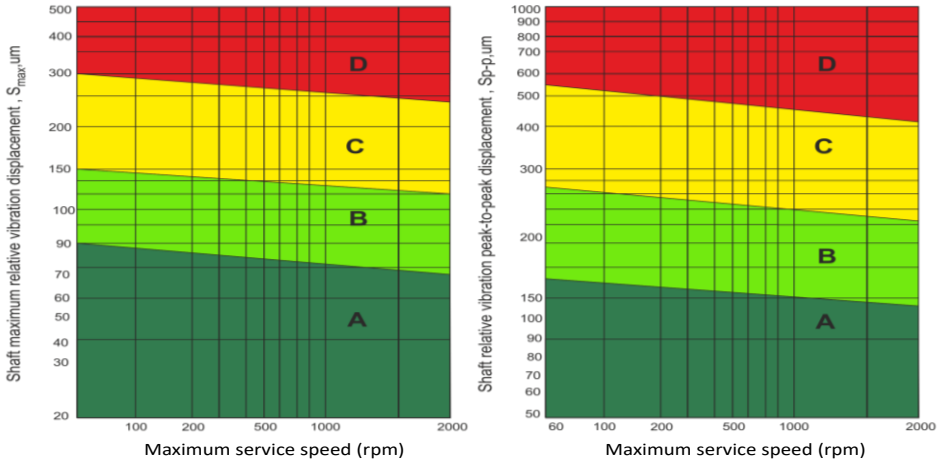

Figure 6. S_{pp} and S_{max} according to ISO 7919-5.

Table 2. Evolution of PAI bearing displacement indicators.

Test	S_{max} (µm)	Exentr. (µm)	S_{p1} (µm)	S_{p2} (µm)	S_{pp} (µm)	GapX (µm)	GapY (µm)
MAVNE	146	1	252	236	284	-1	0
MAVEX	146	10	262	234	289	10	4
20MW	124	25	215	192	242	25	-1
40MW	131	44	229	190	251	39	-21
60MW	109	24	194	167	215	21	-11
80MW	110	11	192	165	215	2	11
40MW +Q	125	39	221	191	244	35	-17
40MW -Q	121	33	219	185	240	28	-18

Table 3. Evolution of PTU bearing displacement indicators.

Test	S_{max} (µm)	Exentr. (µm)	S_{p1} (µm)	S_{p2} (µm)	S_{pp} (µm)	GapX (µm)	GapY (µm)
MAVNE	218	7	310	319	386	-5	4
MAVEX	203	30	331	298	377	19	23
20MW	191	220	327	273	327	-82	-204
40MW	287	266	501	391	502	-129	-233
60MW	170	259	305	214	305	-154	-209
80MW	182	225	347	268	347	-145	-172
40MW +Q	335	202	540	483	550	-95	-178
40MW -Q	305	231	505	460	511	-139	-185

Table 4. Evolution of PAS bearing displacement indicators.

Test	S_{max} (µm)	Exentr. (µm)	S_{p1} (µm)	S_{p2} (µm)	S_{pp} (µm)	GapX (µm)	GapY (µm)
MAVNE	184	8	295	313	351	-2	-8
MAVEX	153	19	249	257	296	-18	4
20MW	143	9	229	236	275	-9	-3
40MW	144	7	236	238	280	-1	-7
60MW	141	35	228	233	272	-34	6
80MW	142	51	241	233	277	-41	30
40MW +Q	147	9	248	238	283	-7	-5
40MW -Q	144	15	238	235	277	-14	5

Table 5. DC level for low frequencies of measuring point 11 RD + PTU.

Test	04 MQUART	05 MDEMI	06 M3QUARTS
Measuring point	11 RD + PTU	11 RD + PTU	11 RD + PTU
DC leval	-7356.0571 (µm eff)	-7414.1113 (µm eff)	-7446.6128 (µm eff)

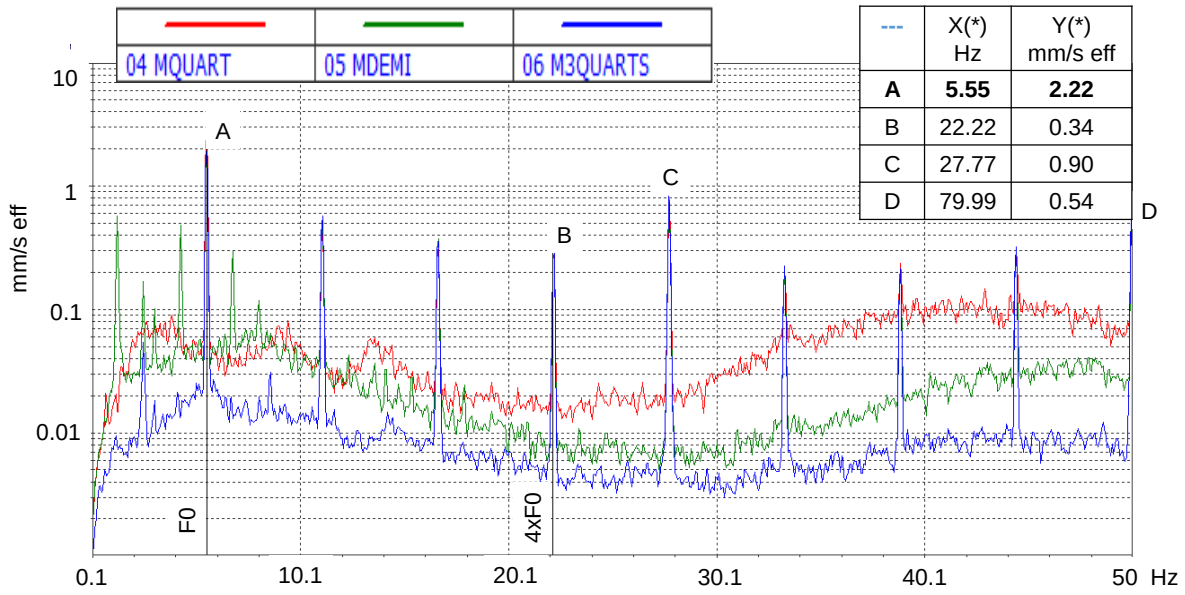

Figure 7. Low frequency spectrum of measuring point 11 RD + PTU.

The PAI bearing displacement measurements reveal satisfactory results. A maximum displacement (S_{pp}) of 289 µm and a maximum peak displacement (S_{max}) of 146 µm are recorded. A very minimal eccentricity is observed throughout the tests, which confirms the stability of the system. Based on ISO 7919-5, these values classify the bearing in zone B. The maximum cumulative displacement reaches a value of order 300 µm. However, it remains below the predefined theoretical tolerance (see Table 6). In this case, it is observed that the shaft line maintains its optimal centering during all operating modes (tests), which also ensures the proper operation of the PAI bearing as for the entire shaft, as explained in Figure 8. This evidence on the behavior of the shaft line guarantees the reliability of the system and its ability to maintain these performances in varied operating conditions.

The displacements recorded at the PAS bearing indicate a peak-to-peak displacement (S_{pp}) of 351 µm, with a maximum displacement recorded (S_{max}) of 184 µm during the maximum full load no-load (MAVNE) tests. In accordance with ISO 7919-5, these measurements classify the bearing in zone C. The maximum cumulative displacement of the shaft in its bearing reaches 360 µm, thus remaining below the theoretical clearance (see Table 7). As with the PAI bearing, the shaft maintains its central position throughout the tests, as shown in Figure 9.

Throughout the acceleration phase, the shaft line remains perfectly centered in its bearings (no offset from the origin), as shown in Figure 10. The displacements of the shaft line are significant, with a total cumulative displacement of approximately 485 µm. More precisely, 305 µm are recorded at the PTU bearing, 305 µm at the PAI bearing, and 628 µm at the PAS bearing (see Table 8). These data highlight the stresses exerted on the different bearings during the acceleration phase, thus emphasizing the importance of careful monitoring of these parameters.

The cumulative displacement of the shaft line measured is of order 477 µm on the PTU bearing, on the PAI bearing is of order 247 µm, and on the PAS bearing is of order 564 µm, as shown in Table 9. Regarding the shutdown process, the shaft line keeps its central position during this phase (normal shutdown signature), as explained in Figure 11. These collected data highlight the capability of the bearings and the stability of the system under both normal conditions, such as start-up and shutdown, which ensures to maintain optimal performance and functional reliability.

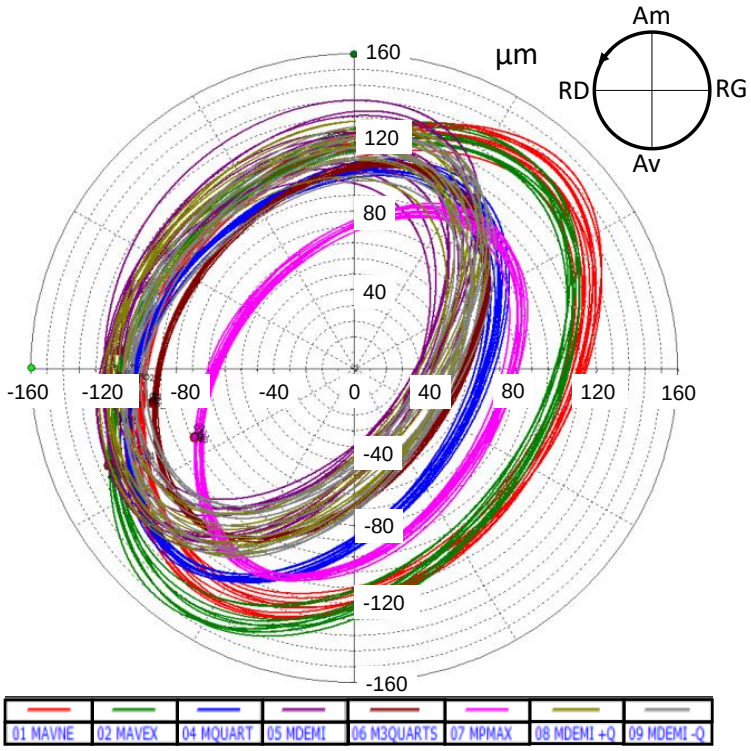

Figure 8. PAI bearing displacement orbits.

Table 6. S_{pp} and S_{max} of measuring point 13 RD + PAI according to the tests.

Test	01 MAVNE	02 MAVEX	03 MQUART	04 MDEMI	05 M3QUARTS	06 MPMAX	07 MDEMI+Q	08 MDEMI -Q
Measuring point	13 RD+PAI	13 RD+PAI	13 RD+PAI	13 RD+PAI	13 RD+PAI	13 RD+PAI	13 RD+PAI	13 RD+PAI
Spp (µm)	283.9518	288.8391	241.5575	250.5909	214.6666	214.6615	243.7117	239.8279
Smax (µm)	146.4131	146.1964	123.8545	130.9628	108.7845	109.5878	125.4384	120.6433

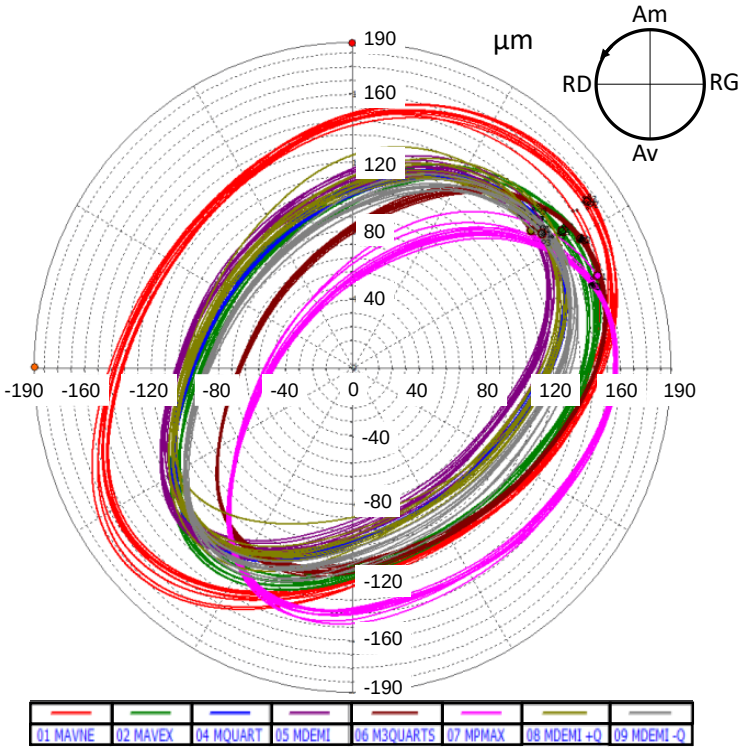

Figure 9. PAS bearing displacement orbits.

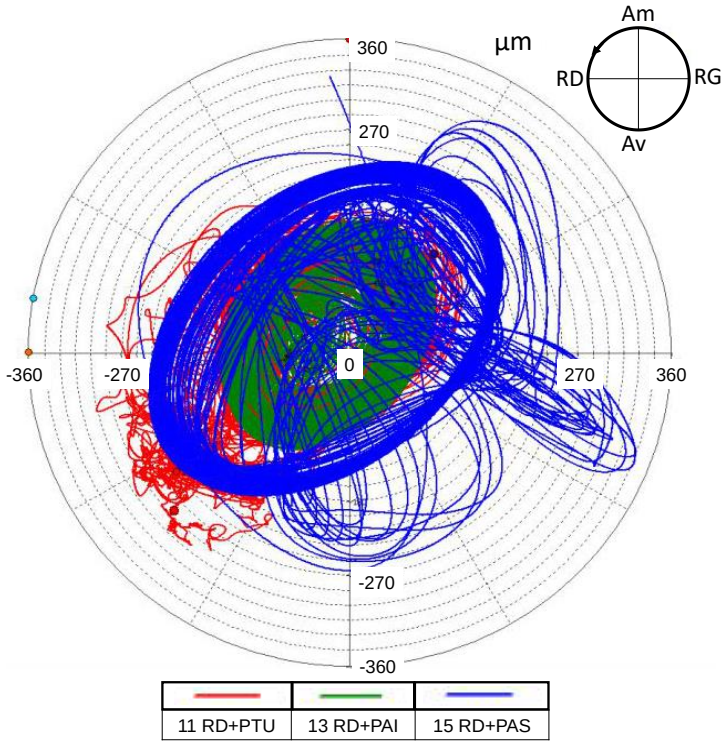

Figure 10. Bearing displacement orbits during start-up.

Table 7. S_{pp} and S_{max} of measuring point 15 RD + PAS according to the tests.

Test	01 MAVNE	02 MAVEX	03 MQUART	04 MDEMI	05 M3QUARTS	06 MPMAX	07 MDEMI+Q	08 MDEMI -Q
Measuring point	15 RD+PAS	15 RD+PAS	15 RD+PAS	15 RD+PAS	15 RD+PAS	15 RD+PAS	15 RD+PAS	15 RD+PAS
Spp (µm)	351.3576	295.5035	275.0793	280.2937	271.7455	276.6647	283.4193	276.6362
Smax (µm)	184.1929	153.2460	142.9217	143.6930	140.9827	141.6541	147.337	143.7225

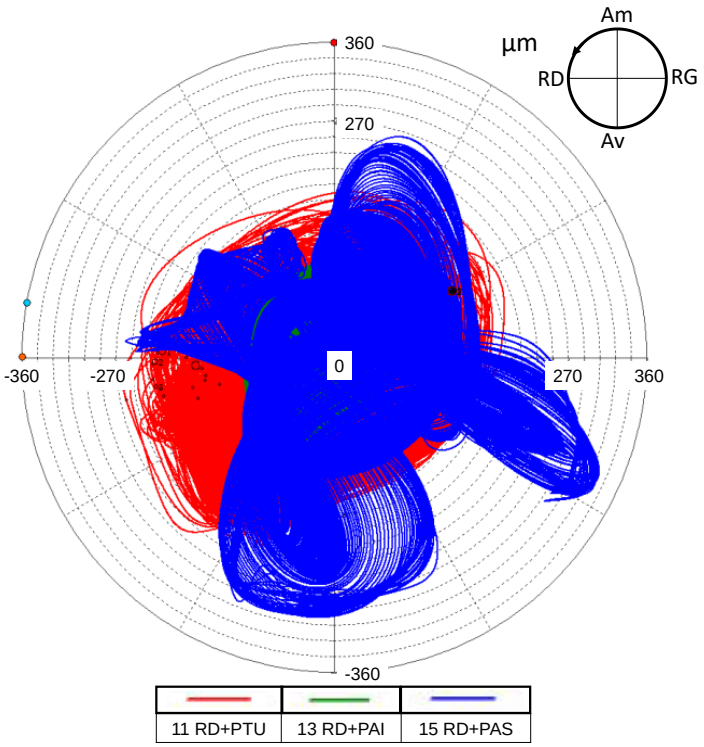

Figure 11. Bearing displacement orbits during normal shutdown.

Table 8. S_{pp} and S_{max} of measuring points 11 RD+PTU, 13 RD+PAI, and 15 RD+PAS of the landings during start-up.

Test	Startup		
Measuring point	11 RD+PTU	13 RD+PAI	15 RD+PAS
Spp (µm)	485.2635	305.2899	628.1533
Smax (µm)	264.8388	166.2438	367.8977

Table 9. S_{pp} and S_{max} of measuring points 11 RD+PTU, 13 RD+PAI, and 15 RD+PAS of the landings during normal stop.

Test	Normal shutdown		
Measuring point	11 RD+PTU	13 RD+PAI	15 RD+PAS
Spp (µm)	477.5346	247.7523	563.7659
Smax (µm)	266.5584	133.0444	307.6003

The treated approach offers remarkable potential for real-time health monitoring, predictive maintenance. Which helps further research works to exploit the robustness and accuracy of the approach in other studies with hydrodynamic bearings of different materials, other rotating machines, reduction of maintenance cost by increasing bearing life, reduction of unplanned failures.

5. Conclusion and Perspectives

This work addressed the problem of shaft line displacements of a hydrodynamic bearing, which can cause failures during operation. It first presents the modeling of the geometric model of the hydrodynamic bearing, as well as the formulation of the boundary condition for proper operation (see equation (16)). Then, a study is conducted to diagnose and evaluate the performance of three PTU, PAI, and PAS bearings of a rotating machine. The adopted approach is based on orbital analysis, compared to the ISO 7919-5 standard. The results obtained using the methodological protocol demonstrate the reliability and accuracy of the diagnostic approach for the different operating tests of the rotating machine. By highlighting a compliant shaft line displacement for:

- The PAI bearing with S_{pp}, S_{max}, and a cumulative displacement of order 289, 146, and 247 µm (respectively), which is lower than the theoretical clearance determined by the manufacturer.
- The PAS bearing with S_{pp}, S_{max}, and cumulative displacement of order 351, 184, and 628 µm (respectively). The cumulative displacement exceeds the theoretical clearance value determined by the manufacturer during start-up, which can cause bearing wear.

  The PAS bearing with S_{pp}, S_{max}, and cumulative displacement of order 485, 305, and 477 µm (respectively).
- The S_{pp} and cumulative displacement exceed the theoretical clearance value determined by the manufacturer during start-up, which can cause bearing wear.

Regarding the shutdown process, the shaft line maintains its central position during this phase (normal shutdown signature). This work opens the way to a relevant research component aimed at setting up a real-

time monitoring system. This system would be based on algorithms integrated into an expert system whose function would be to provide the health status of the hydrodynamic bearing in order to prevent any potential failure. This process would thus contribute to ensuring the reliability and safety of operations while minimizing unforeseen risks; this is given in detail in [36] for the diagnosis and prognosis of a rotating machine based on ANN models.

References

[1] El Adraoui, H. Gziri, A. Mousrij,"Integration of a prognosis model of a rotating microwave oven guidance system subject to linear degradation". In Advances in Integrated Design and Production: Proceedings of the 11th International Conference on Integrated Design and Production, pp. 446-458, 2021, Springer International Publishing. October 14-16, Fez, Morocco, 2019.https://doi.org/10.1007/978-3-030-62199-5_40.

[2] O. T. R. Almeanazel, "Total productive maintenance review and overall equipment effectiveness measurement", Jordan Journal of Mechanical and Industrial Engineering, Vol. 4, No. 4, 2010, pp.517-522.

[3] C. A. A. Rashed, M. N. Bagum, M. M. H. Kibria, R. A. Chowdhury, M. A. Islam, "Integrating Supply Chain Partners through Implementing Industry 4.0 Technologies to Enhance Competitiveness",Jordan Journal of Mechanical and Industrial Engineering, Vol. 81, No. 2, 2024, pp. 351-363. https://doi.org/10.59038/jjmie/180208.

[4] M. Bouaicha, I. El Adraoui, H. Gziri, N. Machkour, M. Zegrari, "Evaluation of the Dynamic Behavior of a Rotor Based on a Vibration Diagnosis". In International Conference on Digital Technologies and Applications pp. 757-766,2022. Cham: Springer International Publishing. https://doi.org/10.1007/978-3-030-62199-5_40.

[5] Adraoui, M. Bouaicha, H. Gziri, M. Zegrari, "Implementation of a diagnostic approach based on vibration analysis: case study of a hydroelectric group", International Journal of Engineering Trends and Technology, Vol. 69, No. 9, 2021, pp.97-106. https://doi.org/10.14445/22315381/IJETT-V69I9P213.

[6] El Adraoui, H. Gziri,A. Mousrij, "Prognosis of a degradable hydraulic system: application on a centrifugal pump", International Journal of Prognostics and Health Management, Vol. 11, No. 2, 2020, pp.1-11. DOI https://doi.org/10.36001/ijphm.2020.v11i2.2926.

[7] X. Yan, C. A. Zhang, Y. Liu, "Multi-branch convolutional neural network with generalized shaft orbit for fault diagnosis of active magnetic bearing-rotor system", Measurement, Vol. 171, 2021, pp. 108778.https://doi.org/10.1016/j.measurement.2020.108778.

[8] G. Bruand, F. Chatelain, P. Granjon, N. Martin, C. Duret, "Reconstructing shaft orbit using angle measurement to detect bearing faults", Mechanical Systems and Signal Processing, Vol. 139, 2020, pp. 106561.https://doi.org/10.1016/j.ymssp.2019.106561.

[9] L. Fan, T. Inoue, A. Heya,Y. Watanabe, "Predicting stability of synchronous nonlinear vibration in vertical rotating shaft system with journal bearing", Journal of Sound and Vibration, Vol. 572, 2024, pp. 118191. https://doi.org/ 10.1016 /j.jsv.2023.118191.

[10] S. Hou, R. Lin, L. Hou, Y. Chen, "Dynamic characteristics of a dual-rotor system with parallel non-concentricity caused by inter-shaft bearing positioning deviation", Mechanism and Machine Theory, Vol. 184, 2023, pp. 105262. https://doi.org/ 10.1016/j.mechmachtheory.2023.105262.

[11] X. Jiang, Z. Wang, Q. Chen, X. Cheng, S. Xu, S. Yang, J. Meng, "An orbit-based encoder–forecaster deep learning method for condition monitoring of large turbomachines", Expert Systems with Applications, Vol. 238, 2024, pp. 122215.https://doi.org/10.1016/j.eswa.2023.122215.

[12] X. Ma, P. K. Wong, J. Zhao, "Practical multi-objective control for automotive semi-active suspension system with nonlinear hydraulic adjustable damper", Mechanical Systems and Signal Processing, Vol. 117, 2019, pp. 667-688.https://doi.org/10.1016/j.ymssp.2018.08.022.

[13] D. F. Shi, W. J. Wang, P. J. Unsworth, L. S. Qu, "Purification and feature extraction of shaft orbits for diagnosing large rotating machinery", Journal of Sound and Vibration, Vol. 279, No.3-5, 2005, pp. 581-600. https://doi.org/10.1016/j.jsv.2003.11.036.

[14] N. A. Saeed, E. M. Awwad, M. A. El-Meligy, E. A. Nasr, "Sensitivity analysis and vibration control of asymmetric nonlinear rotating shaft system utilizing 4-pole AMBs as an actuator", European Journal of Mechanics-A/Solids, Vol. 86, 2021, pp. 104145.https://doi.org/10.1016/j.euromechsol.2020.104145.

[15] X. Cui, J. Huang, C. Li,Y. Zhao, "Three-dimensional instantaneous orbit map for rotor-bearing system based on a novel multivariate complex variational mode decomposition algorithm", Mechanical Systems and Signal Processing, Vol. 178, 2022, pp.109211.https://doi.org/10.1016/j.ymssp.2022.109211.

[16] N. Miloradović, B.Stojanovic, "Tribological behaviour of ZA27/10SiC/1Gr hybrid composite", Journal of the Balkan Tribological Association, 2013.

[17] S. Mitrovic, M. Babic, N. Miloradović, I. Bobic, B. Stojanovic, D. Dzunic, M. Pantić, "Wear characteristics of hybrid composites based on Za27 alloy reinforced with silicon carbide and graphite particles", Tribology in industry, 2014.

[18] Marinković, B. Stojanović, C. Gachot, T. Lazović, "Analysis of Lubrication Regimes for Porous Sliding Bearing", Lubricants, Vol. 12, No. 6, , 2024, pp.184.https://DOI 10.3390/lubricants12060184.

[19] J. Shen, Y. Liu, Y. Zeng,"Axlebox bearing fault diagnosis method for rolling stock combining improved CEEMD and MOMEDA", Diagnostyka, Vol. 25, No. 4, 2024, pp. 1-11. DOI: https://doi.org/10.29354/diag/192497.

[20] Lakikza, H. Cheghib, N. Kahoul, "Optimized variational mode decomposition for improved bearing fault diagnosis and performance evaluation", Archive of Mechanical Engineering, vol. 71, No. 4, 2024, pp. 467-495.DOI: 10.24425/ame.2024.152615.

[21] Y. Bousseloub, F. Medjani, A. Benmassoud, et al. "New method for bearing fault diagnosis based on VMD technique", Diagnostyka, Vol. 25, No. 2, 2024, pp. 1-11.DOI: https://doi.org/10.29354/diag/186751.

[22] Lakikza, H. Cheghib, N. Kahoul,"Diagnosis of bearing faults in wind turbine systems using vibrational signal processing and machine learning", Diagnostyka, Vol. 25, No 3, 2024, pp. 2024307.DOI: https://doi.org/10.29354/diag/191393

[23] S. Xue, I. Howard, C. Wang, H. Bao, P. Lian, G. Chen, et al.,"The diagnostic analysis of the planet bearing faults using the torsional vibration signal", Mechanical systems and signal processing, Vol. 134, 2019, pp. 106304.https: //doi.org/10.1016/j.ymssp.2019.106304.

[24] Y. Chen, H. Zhang, X. Li, D. Shi, Z. Shi, F. Gu, "Wear Parameters Identification of Hydrodynamic Bearing based on Operational Modal Analysis and On-Rotor Sensing Technology", Tribology International, Vol. 198, 2024, pp. 109840.https://doi.org/10.1016/j.triboint.2024.109840.

[25] C. Opia, M. F. B. Abdollah, C. Johnson, F. B. M. Z. SamionSyahrullail, "Lubricity performance evaluation of organic polymer as additives invegetable oil understeel materials",Jordan Journal of Mechanical and Industrial

Engineering, Vol. 17, No. 3, 2023, pp.385-395. https://doi.org/10.59038/jjmie/170307.

[26] F. Abbas, A. E. AL-Kawaz, Z. K. Mezaal, "Studying the Tribological and Mechanical Properties of the PMMA Nano Composite Coating", Jordan Journal of Mechanical and Industrial Engineering, Vol. 8, No. 2, 2024, pp.365-375.https://doi.org/10.59038/jjmie/180209.

[27] R. Venkatesh, "Machining parameter optimization and study the turning operation behavior of hybrid Al/Mg composites",Jordan Journal of Mechanical and Industrial Engineering, Vol. 81, No. 4, 2024, pp. 711-719. https://doi.org/10.59038/jjmie/180407.

[28] V. K. Vasu, K. S. Umashankar, V. Kumar,H. Gouda, "Designing Optimal Parameters Using Taguchi Method for the Tribological Analysis of Al-Si alloy (LM29) Reinforced with Multi-Walled Carbon Nanotubes via the Liquid Metallurgy Route",Jordan Journal of Mechanical and Industrial Engineering, Vol. 81, No.4, 2024, pp. 861- 875. https://doi.org/10.59038/jjmie/180417.

[29] Abdelkawy, E. A. El-Danaf,A. Almajid, "The Effect of Alloying, Processing and Heat Treatment on the Wear Resistance of Al-Cu-Mg-Ag Alloys", Jordan Journal of Mechanical and Industrial Engineering, Vol. 17, No. 2, 2023, pp. 243– 253. https://doi.org/10.59038/jjmie/170208.

[30] M. Bouaicha, M. Guerroum, I. El Adraoui, M. Zegrari, H. Gziri, A. Ait Elmahjoub, "Diagnosis of mechanical faults affecting a hydroelectric group by vibration analysis", International Journal of Emerging Technology and Advanced Engineering, Vol. 11, No. 11, 2021, pp. 86-100. https://doi.org/10.14445/22315381/IJETT-V69I9P213.

[31] L. Licht, M. Branger, "Motion of a Small High – Speed Rotor in 3 types of Foil Bearings", Journal of Lubrication Technology, Vol. 97, No. 2, 1975, pp. 270-280.https://doi.org/10.1115/1.3452571.

[32] N. Arakere, H. D. Nelson, "An Interior Collocation Method for Static and Dynamic Analysis of Finite Length Gas Journal Bearings", Journal of Tribology, Vol 110, No. 3,1988, pp. 456-461.https://doi.org/10.1115/1.3261650.

[33] O. Bonneau, "Static and dynamic behavior of shaft line mounted on fluid bearings: influence of bearing characteristics",Doctoral thesis, Poitiers, 1989.

[34] P. Stephan, "Gas bearings with expandable bore: dynamic behavior",Doctoral thesis, Toulouse 3, 1991.

[35] J. Frene, D. Nicolas, B. Degueurce, D. Berthe, M. Godet, "Hydrodynamic lubrication: bearings and thrust bearings", Elsevier, 1997.

[36] E. Adraoui, Y. Jabari,H. Gziri, "Health Prognosis of a Rotating Rotor Machine with a Pure Unbalance Fault Using an ANN Model", International Review of Mechanical Engineering, Vol. 18, No, 3, 2024, pp. 144–152.DOI: https://doi.org/10.15866/ireme.v18i3.24359.